Canadian Geotechnical Journal

Article

Effect of hydraulic conductivity and impeded drainage on the liquefaction potential of gravelly soils

Jashod Roy and Kyle M. Rollins

Department of Civil and Environmental Engineering, Brigham Young University, 430 Engineering Bldg., Provo, UT 84602, USA

Corresponding author: **Kyle M. Rollins** (email: rollinsk@byu.edu)

Abstract

Investigating the role of sand and fines content and in situ drainage conditions in governing the hydraulic conductivity of gravelly deposits is highly important to characterize the liquefaction potential of gravelly soil. In this study, a variation of hydraulic conductivity with sand content has been empirically obtained based on the existing gravel liquefaction case histories. It is found that the hydraulic conductivity of a soil matrix having more than about 20%–30% sand content by mass is low enough to cause liquefaction without the presence of any impervious confining layer. In addition, a numerical study has been performed using the commercial software FEQDrain to study pore pressure generation in gravelly soil at a variety of relative densities and hydraulic conductivities with and without an impermeable cap layer when subjected to a variety of earthquake loadings. For both unconfined and confined condition, excess pore pressure ratios consistently increase with a decrease in hydraulic conductivity (k) and relative density (D_r). Excess pore pressure ratio is correlated with hydraulic conductivity, soil compressibility, and cyclic stress ratio (CSR). For the confined condition, pore pressure in the gravel layer is primarily governed by the overlying cap layer and even a sandy cap layer instead of highly impervious clay layer can cause liquefaction.

Key words: gravel liquefaction, hydraulic conductivity, sand content, cap layer

Résumé

L'étude du rôle du contenu en sable et en fines et des conditions de drainage in situ dans le contrôle de la conductivité hydraulique des dépôts graveleux est très importante pour caractériser le potentiel de liquéfaction des sols graveleux. Dans cette étude, une variation de la conductivité hydraulique en fonction de la teneur en sable a été obtenue de manière empirique sur la base des cas de liquéfaction de gravier existants. On a constaté que la conductivité hydraulique d'une matrice de sol ayant une teneur en sable supérieure à environ 20-30 % en masse est suffisamment faible pour provoquer une liquéfaction sans la présence d'une couche de confinement imperméable. En outre, une étude numérique a été réalisée à l'aide du logiciel commercial FEQDrain pour étudier la génération de la pression interstitielle dans un sol graveleux à une variété de densités relatives et de conductivités hydrauliques avec et sans couche de couverture imperméable lorsqu'il est soumis à une variété de charges sismiques. Pour les conditions non confinées et confinées, les rapports d'excès de pression de pore augmentent systématiquement avec une diminution de la conductivité hydraulique et de la densité relative. Le rapport de surpression interstitielle est corrélé avec la conductivité hydraulique, la compressibilité du sol et le rapport de contrainte cyclique. Pour la condition confinée, la pression interstitielle dans la couche de gravier est principalement régie par la couche de couverture sus-jacente et même une couche de couverture sableuse au lieu d'une couche d'argile très imperméable peut provoquer une liquéfaction. [Traduit par la Rédaction]

Mots-clés : liquéfaction du gravier, conductivité hydraulique, teneur en sable, couche de couverture

1. Introduction

In the geotechnical engineering field, liquefaction is primarily known to have occurred in deposits of loose sandy soil or sands with some silt content. But over the past 100 years, there have been a significant number of seismic events which, to the surprise of many, also caused liquefaction of gravelly deposits around the world as shown in Table 1. These incidents of gravel liquefaction have been of great interest for geotechnical engineers and researchers as gravelly soil is not typically expected to liquefy because its hydraulic conductivity is considered to be much higher than sandy soil. This reduces the chance of pore pressure generation during seismic loading even for loosely deposited soil strata. For example, Seed et al. (1976), based on numerical modeling, found that soils with a hydraulic conductivity greater than 0.004 $m \cdot s^{-1}$ would dissipate excess pore pressures as fast as they could be generated by an earthquake and would, therefore, not be susceptible to liquefaction.

Table 1. Case histories involving liquefaction of gravelly soil.

Earthquake	Year	M_w	Reference
Mino-Owari, Japan	1891	7.9	Tokimatsu and Yoshimi (1983)
Fukui, Japan	1948	7.3	Ishihara (1985)
Alaska	1964	9.2	Coulter and Migliaccio (1966), McCulloch and Bonilla (1970)
Haicheng, China	1975	7.3	Wang (1984)
Tangshan, China	1976	7.8	Wang (1984)
Friuli, Italy	1976	6.4	Sirovich (1996*a*, 1996*b*), Rollins et al. (2020)
Miyagiken-Oki, Japan	1978	7.4	Tokimatsu and Yoshimi (1983)
Borah Peak, Idaho	1985	6.9	Youd et al. (1985), Andrus (1994)
Armenia	1988	6.8	Yegian et al. (1988)
Roermond, Netherlands	1992	5.8	Maurenbrecher et al. (1995)
Hokkaido, Japan	1993	7.8	Kokusho et al. (1995)
Kobe, Japan	1995	7.2	Kokusho and Yoshida (1997)
chi-Chi, Taiwan	1999	7.8	Chu et al. (2000)
Wenchuan, China	2008	7.9	Cao et al. (2013)
Cephalonia Is., Greece	2014	6.1	Nikolaou et al. (2014), Athanasopoulos-Zekkos et al. (2019)
Muisne, Ecuador	2016	7.8	Lopez et al. (2018)
Kaikoura, New Zealand	2016	7.8	Cubrinovski et al. (2017)

While the potential for liquefaction of sandy gravel mixtures has been investigated with cyclic triaxial tests (Wong et al. 1974; Banerjee 1979; Evans and Seed 1987; Hynes 1988; Hatanaka et al. 1997; Kokusho et al. 2004) and cyclic simple shear tests (Chang et al. 2014; Hubler et al. 2017), all these tests have simulated undrained conditions. Kokusho et al. (2004) reported that the liquefaction resistance of granular soil can be roughly estimated from the relative density (D_r), despite having significant differences in particle size distribution. Chang et al. (2014) performed cyclic simple shear tests on gravel–sand mixtures and reported that gravel–sand mixtures can be categorized as sand-like, gravel-like, or in-transition mixtures depending on the amount of gravel content. The gravel content in an in-transition-type mixture remains in the range of 30%–60%. If the gravel content remains below this threshold range of 30%–60%, the gravel particles typically float in the gravelly sand matrix, and hence this is considered as a sand-like mixture. Chang et al. (2014) contend that the liquefaction resistance of such sand-like mixtures can be evaluated based on the liquefaction resistance of sand with a correction factor for the gravel content. Based on monotonic and cyclic simple shear tests on sand–gravel mixtures, Hubler et al. (2017) found that the liquefaction resistance was the greatest at an optimum mixture of sand and gravel (60% sand mixed with 40% gravel) compared with the 100% uniform gravel or sand specimens. At the optimum mixture, the void ratio was found to be the lowest leading to higher dry density and liquefaction resistance. Hubler et al. (2017) also found that particle angularity had a significant effect on the monotonic and cyclic response, where subrounded gravelly mixtures had higher liquefaction resistance than rounded gravelly soil.

Researchers have also developed in situ methods of assessing gravel liquefaction to avoid the difficulty of extracting undisturbed gravelly samples for laboratory testing. The typical standard penetration test (SPT) and cone penetration test (CPT) methods have the potential of obtaining artificially high penetration resistance due to the interference with large gravel size particles relative to the penetrometer diameter. However, Idriss and Boulanger (2008) recommended correction of SPT blowcount affected by the interference with relatively large gravel particle based on an inch-by-inch cumulative blowcount measurement with depth. This correction method was also used by Andrus (1994) at the Borah Peak sites for evaluating the liquefaction potential of gravelly deposits.

To overcome the interference with large particles, 168-mm diameter Becker penetration test (BPT) (Harder and Seed 1986; De Jong et al. 2017) has been used and the BPT blowcount was correlated with SPT blowcount for liquefaction assessment. Recently, a 74-mm diameter Dynamic Cone Penetration Test (DPT) (Cao et al. 2013; Rollins et al. 2021) has been correlated with the liquefaction potential of gravelly soil for a wide range of case history data. Besides these penetration tests, efforts have been made to correlate the in situ density of gravelly soil and liquefaction resistance with geophysical measurements i.e., in situ shear wave velocity (V_s) of gravelly deposits (Andrus et al. 1999; Chang 2016). However, none of these in situ methods evaluate the hydraulic conductivity of the gravelly layer as part of the liquefaction assessment. Chen et al. (2018) further investigated the characteristics of the soil deposits at the Chengdu plain in China, and reported that the presence of an impermeable capping layer overlying a loose gravelly deposit can create a highly favorable condition for triggering liquefaction in the gravel layer. In this case, the overall hydraulic conductivity of the soil strata would become too low for rapid dissipation of pore pressure during seismic loading. Chen et al. (2018) also suggested that the existence of an unsaturated gap zone below the clay cap and above the saturated gravelly soil can be an important factor that reduces the chance of liquefaction. The unsaturated gap layer apparently provides

pore pressure dissipation because of the potential for upward drainage.

Despite various studies on liquefaction of gravelly soil, the roles of hydraulic conductivity and drainage boundary conditions in causing liquefaction are not yet well understood, even though these parameters are very significant in controlling pore pressure generation during earthquakes. Although Chen et al. (2018) have provided some insight regarding the effect of an impermeable cap and the unsaturated gap zone on the liquefaction potential of a gravel layer, no conclusive remarks were provided from a design perspective. In addition, there are several incidents where gravel liquefied without the presence of any impermeable cap layer, e.g., the 1985 Borah Peak earthquake in Idaho, the 1964 Alaska earthquake, and the 2014 Cephalonia earthquake in Lixouri and Argostoli that contradict the mechanism of gravel liquefaction suggested by Chen et al. (2018). These observations also give rise to the possibility that soils classifying as gravel according to the Unified Soil Classification System (USCS), for example, may behave like sand, because of the low range of hydraulic conductivity produced by the sand content in the soil matrix.

In this study, an effort has been made to investigate the range of hydraulic conductivity of the liquefied and nonliquefied gravelly soils from the case history data available in the literature in relation to their grain-size characteristics. Furthermore, extensive numerical analyses have been performed using FEQDrain (Pestana et al. 1997) to analyze the pore pressure generation of gravelly soil over a wide range of seismic loadings and hydraulic conductivities with various drainage conditions. Finally, conclusions have been drawn regarding the effect of various drainage parameters on the liquefaction of gravelly soil, e.g., thickness of impermeable cap layer, unsaturated gap zone, hydraulic conductivity, percentage of sand and gravel fractions in the soil matrix, particle size distribution, and porosity with the goal of providing important insight for design practice.

2. Hydraulic conductivity analysis of gravelly deposits based on case history data

The existing literature on gravel liquefaction, as referenced in Table 1, includes site investigation results for several sites across the world where gravelly soils did or did not liquefy during various seismic events. In the present study, the grain-size distribution curves of the gravelly strata for these sites have been collected and the hydraulic conductivity has been estimated using empirical correlations. Average gradation curves for each of these sites are shown in Fig. 1 to demonstrate the range of gradations of the potentially liquefiable gravelly deposits around the world. Fig. 1 shows that the liquefied and nonliquefied gravelly deposits consist of a wide range of particle size distributions varying from a very poorly graded to a well-graded soil matrix.

To estimate the hydraulic conductivity (k) for each site, the Kozeny–Carman relationship (Kozeny 1927; Carman 1936, 1956) has been used as given by eq. 1.

$$(1) \quad k = \frac{g}{\nu}\left(8.3 \times 10^{-3}\right)\left[\frac{n^3}{(1-n)^2}\right]D_{10}^2$$

where k is in units of metre per second, n is the porosity, D_{10} is the grain size diameter (mm) for which 10% is finer, ν is the kinematic viscosity of water, and g is the acceleration of gravity.

Carrier (2003) reported that the Kozeny–Carman equation would not be applicable for granular soils with effective sizes greater than 3 mm or clayey soil (Odong 2007). However, the accuracy of this equation for gravelly soil with a broad particle size distribution is greater than the other well-known formulations such as Hazen (1892), which is primarily used for sand. The approximate porosity (n) has been computed from the gradation curve for each gravelly site using the empirical relationship given by eq. 2, which was proposed by Milan and Andjelko (1992),

$$(2) \quad n = 0.255\left(1 + 0.83^{C_u}\right)$$

where C_u is the uniformity coefficient defined as D_{60}/D_{10}. D_{60} and D_{10} can be obtained from the gradation curve as D_{60} and D_{10} are grain size diameters for which 60% and 10% are finer, respectively. Based on eqs. 1 and 2, the hydraulic conductivity is governed by the porosity and grain-size distribution characteristics.

The Supplementary Table S1 provides a summary of the case history information including the salient properties from the gradation curves (D_{60}, D_{30}, D_{10}, C_u, C_c) along with the k and n values obtained by eqs. 1 and 2 for all the sites considered in the present study. Besides the hydraulic conductivity, the percentage of sand in the gravelly soil matrix is considered to be another significant parameter controlling the drainage characteristics of gravelly deposits during earthquake loading (Evans and Zhou 1995; Hubbler et al. 2017). Therefore, the sand percentage for every site has also been obtained from the gradation curve and listed in Supplementary Table S1.

It can be observed from Supplementary Table S1 that the sand content varies from 20% to 90% for the whole data set and 80% of the data set has a sand content greater than 30%. The uniformity coefficient (C_u) and the coefficient of curvature (C_c) vary from 5.2 to 475 and 0.028 to 154.3, respectively, indicating a wide distribution of particle sizes for the gravelly deposits, which liquefied in past earthquakes. The wide range of particle size distributions for the gravelly sites in the case histories is also confirmed by the wide variation of the D_{60}, D_{30}, and D_{10} values shown in Supplementary Table S1. Because of the variation of particle size, the hydraulic conductivity of the soil matrix computed using eq. 1 also seems to vary significantly from a lower range of 4×10^{-6} m·s^{-1} to an upper range of 3×10^{-3} m·s^{-1}. However, for all the case histories, the hydraulic conductivity is lower than the boundary defined by Seed et al. (1976) for liquefaction susceptibility ($k < 4 \times 10^{-3}$ m·s^{-1}).

To date, several studies have indicated that the sand content plays a significant role in determining the hydraulic con-

Fig. 1. Grain size distribution of liquefied gravelly sites. [Color online.]

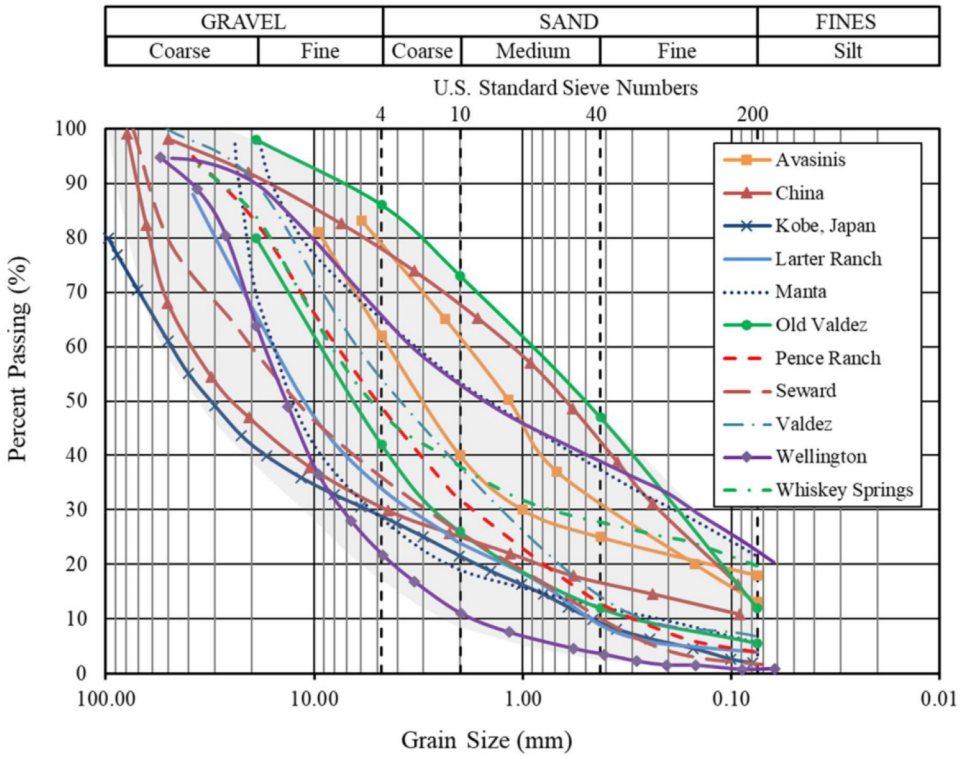

ductivity of sand–gravel mixtures. Based on experimental results, Mason et al. (1997) showed that as the sand content increases, the hydraulic conductivity of the sand–gravel mixture decreases very rapidly and reaches a value that approximates that of pure sand at a sand content of 30%–40%. Lopez de San Román-Blanco (2003) further provided experimental results, which showed a similar variation in porosity as sand content increased. The results of Mason (1997) and Román-Blanco (2003) suggest that the presence of a sufficient sand content can dramatically alter the hydraulic conductivity of the sediment in contrast to that of pure gravel. This observation suggests that sand content could govern the potential for liquefaction by controlling the drainage characteristics of the gravelly deposits and the corresponding pore pressure generation during the seismic loading (Seed et al. 1975*a*).

She et al. (2006) developed a theoretical relationship between the porosity, sand content, and hydraulic conductivity for sand–gravel mixtures. These relationships were also validated with results obtained from laboratory experiments. Based on this investigation, She et al. (2006) developed the curves, depicted in Fig. 2, to show the variation of hydraulic conductivity with the percentage of sand for coarse, medium, and fine sand–gravel mixtures using the concept of "under-filled", "fully-filled", and "over-filled" mixtures. The "under-filled" mix is where the sand fraction is insufficient to fill the pore space between the gravel particles, while the "over-filled" mix is where there is more sand than that required to fill up the gravel pore space. The "fully-filled" is that case where the sand fraction is just sufficient to fill the void space in the gravel.

It can be observed from Fig. 2 that as the sand content decreases below 32%, the hydraulic conductivity increases rapidly for coarse, medium, and fine sand mixtures as the sand–gravel mixtures remain under-filled with a high porosity and the k value for all three soil mixtures roughly coincide with each other. But as the sand content increases above 30%–32%, the mixture becomes over-filled, and the hydraulic conductivity remains relatively constant with a value depending on the grain size of the sand, i.e., coarse, medium, or fine. The transition zone between the under-filled and over-filled mixture represents the fully filled mixture. Although the concept of "under-filled", "fully-filled", and "over-filled" mixtures were first hypothesized by Lopez de San Román-Blanco (2003) to demonstrate the variation of porosity of sand–gravel mixture with the sand content, She et al. (2006) extended the concept to investigate the effect on the hydraulic conductivity. The liquefaction susceptibility boundary suggested by Seed et al. (1976) is also shown in Fig. 2.

In the present study, the empirically obtained hydraulic conductivity values of the gravelly soils for the available gravel liquefaction field case histories have been plotted with respect to the corresponding sand content in Fig. 2 along with the theoretical curves produced by She et al. (2006). Besides these empirically obtained hydraulic conductivity values in Supplementary Table S1, a significant number of hydraulic conductivity values have been measured in situ at several liquefaction and no-liquefaction sites on the Chengdu plain in China in the 2008 Wenchuan earthquake (Zhou et al. 2020). These measured k values are also plotted in Fig. 2 for direct comparison with the empirical database and theoret-

Fig. 2. Variation of hydraulic conductivity of sand–gravel mixtures with the sand content for fine to coarse sands as suggested by She et al. (2006) along with liquefaction and nonliquefaction data points from field case histories. [Color online.]

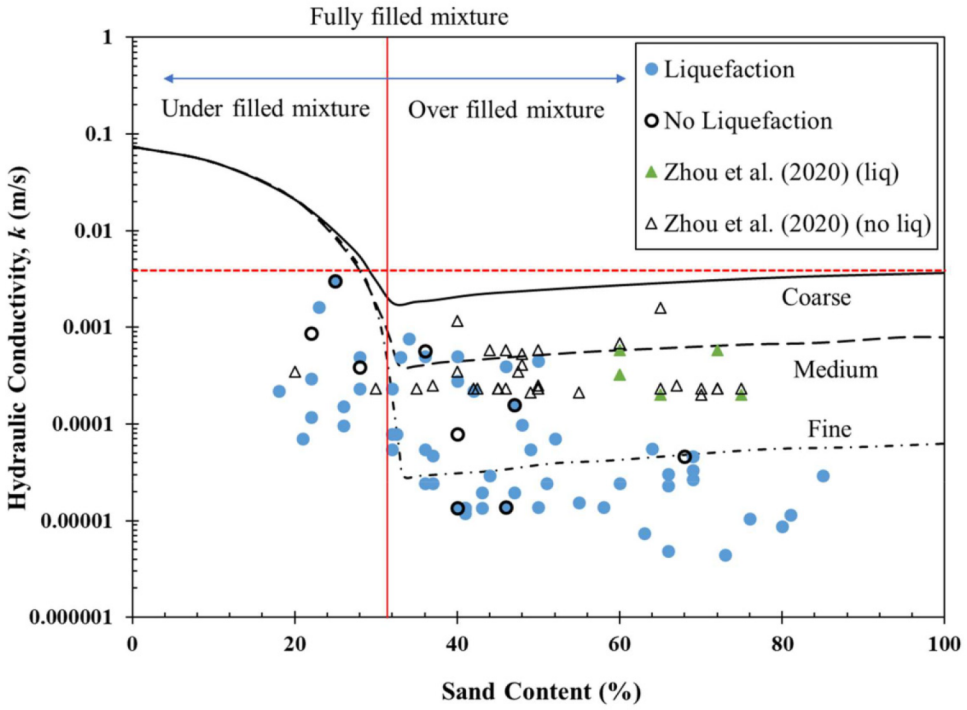

ical curves of She et al. (2006). The comparison shows that the hydraulic conductivity values of all the case history data points are well distributed through the coarse, medium, and fine sand mixture lines. Most of the liquefaction points fall below the medium and fine sand mixture lines in the over-filled zone. There are a few liquefaction and no-liquefaction points that remain close to the boundary between the fully filled and under-filled zones, but the hydraulic conductivity still remains less than the expected value of under-filled line. This can be due to variations in the compaction level and corresponding relative density of the gravelly deposits compared with the theoretical curves. She et al. (2006) reported that higher levels of compaction and consolidation during the deposition of the sandy gravel can significantly reduce the porosity as well as the hydraulic conductivity of the soil matrix. Consequently, the critical sand content of the fully filled mixture at the transition zone will also be reduced a considerable amount with lower porosity. Thus, the hydraulic conductivity of the gravelly deposit can be relatively low even for an under-filled soil matrix having a lower sand content if the soil matrix remains well compacted with a higher relative density.

A large number of no-liquefaction points from the Zhou et al. (2020) database, which are based on in situ measurement fall near the medium sand–gravel mixture line, indicating higher permeability compared with the empirically obtained liquefaction points even when the sand content is much higher than 30%. However, these no liquefaction points are still much below the coarse mixture or even the threshold line of 0.004 m s^{-1}, suggested by Seed et al. (1976). Also, there are a few empirically obtained no-liquefaction points near or below the fine mixture line, which should be susceptible to liquefaction triggering. Although the liquefaction points are explained well by the corresponding range of hydraulic conductivity values in Fig. 2, the presence of no-liquefaction points between medium and fine mixture line in the over-filled zone indicates that the liquefaction potential is a function of several other factors besides hydraulic conductivity. For example, gravelly deposits with high relative density may have a cyclic resistance ratio (CRR) higher than the cyclic stress ratio (CSR) produced by the earthquake event, and therefore not experience liquefaction despite having low hydraulic conductivity due to high sand content.

Besides the hydraulic conductivity of the gravel layer, the presence of an impermeable (clay) cap layer overlying the gravelly deposit or an unsaturated permeable gap zone above the water table may also play a significant role in controlling the hydraulic conductivity of the overall soil deposit and eventually the generation of pore pressure during seismic loading as suggested by Chen et al. (2018). The data summary given in Supplementary Table S1 also includes information regarding the presence of an impermeable cap layer and the unsaturated gap layer for the available case history sites. The present database shows that there are several cases where liquefaction took place without any cap layer. This appears to have occurred because the sand and silt content was high enough to reduce the hydraulic conductivity of the sandy gravel layer to that of sand.

There are also several cases such as the Wellington port in New Zealand where liquefaction did not take place despite having a concrete cap layer on top of the gravelly deposit. As noted previously, this is likely due to the lower CSR produced

by these smaller magnitude earthquakes compared with the CSR required to cause liquefaction. Although the hydraulic conductivity of the gravelly deposit along with the drainage boundary conditions may have a significant effect on liquefaction susceptibility, ultimately the occurrence of liquefaction depends on the combination of the earthquake loading in comparison to the penetration resistance (or relative density) of the soil.

Unfortunately, the available case history database is insufficient to provide overall conclusions regarding the combined effect of relative density, hydraulic conductivity, and drainage boundary conditions. Therefore, to investigate the effect of all these parameters together, a detailed parametric study has been performed in the present study using the numerical model in FEQDrain (Pestana et al. 1997) to compute the generation of excess pore pressure for a variety of intensities of earthquake shaking for soil layers with variable relative densities, hydraulic conductivities, and drainage boundary conditions.

3. Numerical study

The program FEQDrain was originally developed by Pestana et al. (1997) to compute the influence of vertical drains in reducing the potential for excess pore pressure generation in a soil stratum under earthquake shaking. However, in this case, the program was used to consider the generation and dissipation of pore water in a soil layer through vertical drainage only. A finite element modeling technique is used to discretize the soil profile and drainage boundaries. The basic assumptions lying behind the analysis method are: (1) continuity of flow and that flow is governed by Darcy's law, (2) the soil is completely saturated, and (3) the change in porosity due to seismically induced compression is equivalent to the change in volumetric strain. Based on these assumptions, the primary equation governing the generation of pore pressure under seismic loading can be given by

$$(3)\qquad \left(\nabla k\frac{\nabla u}{\gamma_w}\right) = m_v\left(\frac{\partial u}{\partial t} - \frac{\partial u_g}{\partial t}\right)$$

developed by Pestana et al. (1997), where k is the hydraulic conductivity, u is the pore pressure, ∇ is the space gradient operator, γ_w is the unit weight of water, m_v is the coefficient of volumetric compressibility, u_g is the excess pore pressure generated by cyclic loading, and t is the elapsed time.

Pore pressure generation by cyclic loading (u_g) is modeled in FEQDrain by transforming irregular seismic loading into an equivalent number of uniform cycles occurring within a specified length of time, as described by Seed et al. (1975*a*) using eqs. 4 and 5

$$(4)\qquad \frac{\partial u_g}{\partial t} = \frac{\partial u_g}{\partial N}\frac{\partial N}{\partial t}$$

$$(5)\qquad \frac{\partial N}{\partial t} = \frac{N_{eq}}{t_d}\quad (\text{for}\quad 0 < t \le t_d);\ \frac{\partial N}{\partial t} = 0\quad (\text{for}\quad t > t_d)$$

where N is the accumulated number of cycles at time t, N_{eq} is the equivalent number of uniform cycles, and t_d is the time period of shaking (typically equivalent to time of strong motion).

Extensive laboratory testing using cyclic triaxial and simple shear tests has shown that the relationship between u_g and N can be expressed by

$$(6)\qquad R_u = \frac{u_g}{\sigma_0'} = \frac{2}{\pi}\arcsin\left(\frac{N}{N_l}\right)^{\frac{1}{2\theta}}$$

where R_u = excess pore pressure ratio, σ_0' = initial mean effective stress under triaxial conditions or the initial vertical stress for simple shear conditions, N_l = number of uniform stress cycles causing liquefaction in a cyclic undrained test, and θ = an empirical constant, typically equal to 0.7. Substituting eqs. 5 and 6 into eq. 3, the rate of excess pore pressure generation takes the following form:

$$(7)\qquad \frac{\partial u_g}{\partial t} = \frac{\sigma_0'}{\theta\pi}\left(\frac{N_{eq}}{N_l t_d}\right)\frac{\tan\left(\frac{\pi R_u}{2}\right)}{\sin^{2\theta}\left(\frac{\pi R_u}{2}\right)}$$

Variation of the excess pore pressure ratio (R_u) with the cycle ratio (N/N_l) obtained from cyclic triaxial and cyclic simple shear tests (Lee and Albasia 1974; DeAlba et al. 1975) including the Seed et al. (1975a) model is shown in Fig. 3.

The volumetric compressibility (m_v) is obtained using the following equation developed by Seed et al. (1975*a*)

$$(8)\qquad \frac{m_v}{m_{v0}} = \frac{\exp(y)}{1 + y + \frac{y^2}{2}} \ge 1$$

where $y = aR_u^{b}$; $a = 5(1.5 - D_r)$; $b = 3(4)^{-D_r}$; D_r is the initial relative density; m_{vo} is the initial value of volumetric compressibility ($\Delta\varepsilon/\Delta\sigma'$).

The hydraulic conductivity matrix depends on the discretization of the soil strata and the external drainage boundary, if any, used in the numerical modeling. However, details of the finite element formulation along with the element integration to obtain the excess pore pressure generation can be found in the FEQDrain manual by Pestana et al. (1997).

In this study, two different kinds of gravel deposits have been considered—one having only an unconfined sandy gravel layer with the water table at the surface level and the other consisting of the same uniform sandy gravel deposit confined by an overlying lower hydraulic conductivity layer with the water table remaining below the top layer. In the confined condition, the cap layer acts as a drainage provision and hence it has been kept dry above the water table to allow dissipation of pore pressure from the underlying gravel layer. The entire soil strata have been subjected to seismic loadings of various magnitudes in terms of equivalent loading cycles (N_{eq}) and duration of shaking (t_d) according to recommendations by Seed and Idriss (1982). While running the analysis for seismic loading, the initial static water table was kept constant for each run and drainage was only allowed in the vertical direction. No horizontal drainage was considered due to installation of a composite prefabricated vertical (PV)

Fig. 3. Variation of excess pore pressure ratio (R_u) with cycle ratio (N/N_l). [Color online.]

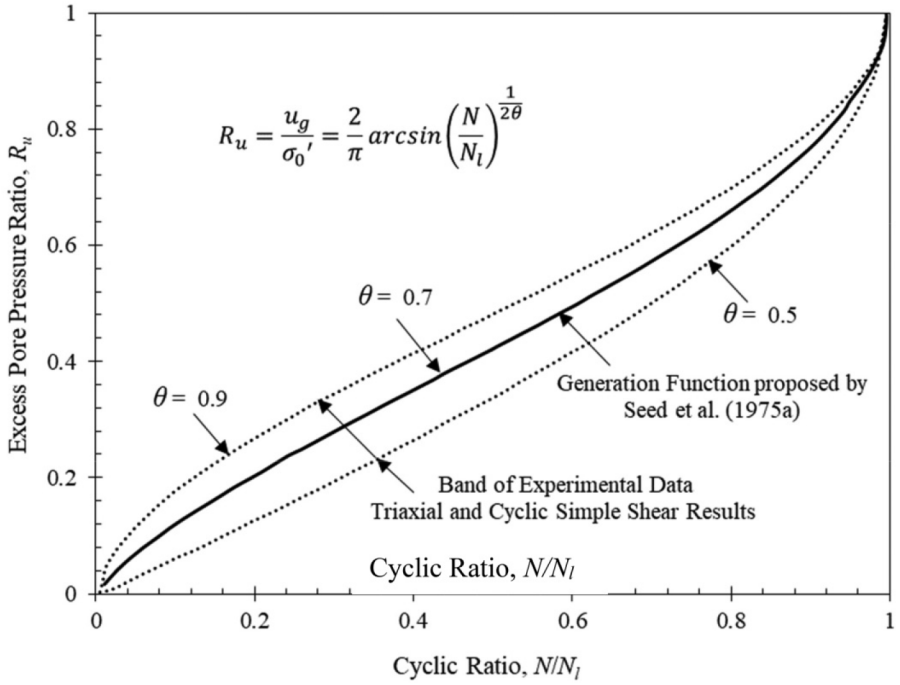

drainage system in the soil model. The soil layers have been discretized in such a way that each vertical increment has the thickness of 0.076 m, whereas horizontal discretization has been ignored. Thus, the set of analyses performed in the present study essentially represents a one-dimensional analysis. Based on this numerical set up, a detailed parametric study has been performed to understand the effect of various parameters such as hydraulic conductivity, earthquake magnitude, and soil density on the generation of pore pressure under different drainage conditions during earthquake shaking. The details regarding the selection of all the input parameters to simulate various earthquake loading conditions and soil characteristics are described in the following sections.

3.1. Coefficient of hydraulic conductivity

Based on the field case history data described previously, the coefficient of vertical hydraulic conductivity of sandy gravel layer has been varied from 6×10^{-3} and 3×10^{-6} m·s^{-1} to include the complete range of available case history data. Consideration of this wide range of hydraulic conductivity also includes the effect of sand content as the hydraulic conductivity of gravelly soil can be significantly controlled by the fraction of sand present in the soil deposit as shown in Fig. 2.

3.2. Relative density

To consider a reasonable range of soil stiffness, the D_r of the gravelly stratum has been varied from 0.2 to 0.5 with an increment of 0.1. Recently, Rollins et al. (2020) has reported a correlation between the DPT resistance (N'_{120}) and the relative density of gravelly soil as given by,

$$(9) \quad D_r = \sqrt{\frac{N'_{120}}{70}}$$

where N'_{120} is the DPT blow counts obtained for 30-cm penetration of DPT cone by using a 120 kg hammer with an average energy efficiency of 89% and further corrected to an overburden pressure of 100 kPa.

3.3. Coefficient of volumetric compressibility

The volumetric compressibility of the sandy gravel layer has been estimated based on a relative view to the stiffness property of gravels in comparison to the same for sands. Seed and Idriss (1970) expressed the shear modulus of granular soil (G) as a function of effective confining stress by the following equation:

$$(10) \quad G = 1000K_2\sqrt{\sigma'_0}$$

where K_2 is an empirical soil modulus coefficient that is a function of void ratio (e) and soil unit weight (γ). The value of K_2 at small strain reaches a maximum, which is symbolized as $(K_2)_{max}$. Seed et al. (1986) reported that the value of $(K_2)_{max}$ is 1.35 to 2.5 times higher for gravels than for sands. This coefficient primarily depends on the relative density of the soil deposit. As the shear modulus of the gravels is roughly two times higher than the sand, the bulk modulus for gravelly soil would also be around two times higher than sand. Therefore, the volumetric compressibility of gravelly soil can be considered as two times lower than the compressibility of sand. Pestana et al. (1997) reported that the compressibility (m_v) of sand approximately varies from 4.1×10^{-7} to 2.05×10^{-7} m^2·kN^{-1} for loose to dense sand according to Lee and Albaisa (1974). Therefore, m_v values for gravelly soil in the present study have been varied from 2.05×10^{-7} to 1.024×10^{-7}

Table 2. Equivalent number of cycles to cause liquefaction for the assumed relative density.

Relative density, D_r	N_l
0.2	4
0.3	6
0.4	10
0.5	30

$m^2 \cdot kN^{-1}$ with an increment of 0.166×10^{-6} $m^2 \cdot kN^{-1}$ for the assumed range of soil density.

3.4. Number of cycles for initial liquefaction

The minimum number of cycles required to initiate liquefaction (N_l) has been obtained by using the procedure based on the stress ratio (τ/τ_1) versus N_l curve as described in Seed and Idriss (1982). To use this method, the applied stress ratio in the form of seismic loading and the corresponding factor of safety for any relative density have to be known. Hence, in the present study, an applied CSR has been assumed for all earthquake magnitudes. For that assumed stress ratio, the factor of safety has been obtained for each relative density (D_r of 0.2–0.5) by using the formulation of CRR/CSR where the CRR has been obtained by using the recently developed DPT-based triggering procedure of Rollins et al. (2021). To obtain the CRR, the equivalent DPT resistance (N'_{120}) for each relative density has been obtained by eq. 9. Then, the assumed stress ratio is divided by this factor of safety value and based on this factored stress ratio value, corresponding N_l is determined from the stress ratio (τ/τ_1) versus N_l curve of Seed and Idriss (1982). It should be noted that the CSR versus N_l curve that is given in Seed and Idriss (1982) is basically the Magnitude Scaling Factor (MSF) curve that was originally developed for the liquefaction of sandy soil. Although several other MSF curves besides the Seed and Idriss (1982) curve have been developed to date, e.g., Idriss (1999), Andrus and Stokoe (2000), Idriss and Boulanger (2008), Kayen et al. (2013), all of these MSF curves have been developed for liquefaction of sand, not for gravelly soil. Hence, in the present study, the N_l values obtained based on Seed and Idriss (1982) procedure have been corrected by the recently proposed *MSF* of Rollins et al. (2021) to obtain the equivalent N_l for gravelly soil. The corrected values of N_l obtained for the assumed range of relative densities in the present study have been summarized in Table 2.

3.5. Number of equivalent cycles

This is essentially an earthquake loading parameter by which a certain magnitude of earthquake with known peak ground acceleration (PGA) is replaced by an equivalent number of cycles at 65% of maximum shear stress (τ_{max}). Seed and Idriss (1982) recommended the values of N_{eq} for a set of earthquake magnitudes as shown in Table 3. These values have been used in the present analysis while performing the parametric study for an assumed range of earthquake magnitudes.

Table 3. Equivalent number of cycles due to earthquake loading (Seed and Idriss 1982).

Magnitude	N_{eq}
5.25	2–3
6	5–6
6.75	10
7.5	15
8.25	26

Table 4. Duration of earthquake strong motions (Seed et al. 1975*b*).

Magnitude	Duration, t_d (s)
5.25–6	8
6.5	14
7	20
7.5	40
8	60

3.6. Duration of earthquake shaking

The value of t_d is based on the duration of strong motion or the bracketed duration (Bolt 1973) and typical values corresponding to the various earthquake magnitudes are given in Table 4 according to Seed et al. (1975*b*). Duration of shaking is also used as an input parameter for earthquake loading.

4. Results of numerical analysis for unconfined gravel layer (without overlying cap)

For this case, a 5-m thick sandy gravel deposit has been considered with relative densities (D_r) of 0.2, 0.3, 0.4, and 0.5 when subjected to earthquakes ranging in magnitude (M_w) from 5.25 to 8.25 with an increment of 0.75. For each of these cases, the maximum R_u has been computed for the sandy gravel stratum as a function of the hydraulic conductivity of the gravel stratum as shown in Fig. 4. Based on these results, several conclusions can be drawn regarding the effect of the various input parameters on the excess pore pressure generation characteristics of the sandy gravel layer.

4.1. Effect of hydraulic conductivity

Figure 4 shows that the peak excess pore pressure ratio (R_u) for a given relative density (D_r) remains very low (in the range of 0.05–0.15) for all earthquake magnitudes when the hydraulic conductivity is typically above a threshold value, which lies in the range of 0.001–0.002 $m \cdot s^{-1}$ depending on the relative density of the soil matrix. Threshold value of k basically indicates that point below which R_u starts increasing rapidly but with a different rate for different earthquake magnitudes and above this point the R_u remains very low (<0.05–0.15) and similar for all magnitudes. However, as the hydraulic conductivity decreases below this range, the peak R_u value begins to increase rapidly and continues un-

Fig. 4. Variation of computed peak excess pore pressure ratio (R_u) within a 5-m thick unconfined gravel layer with relative densities (D_r) of (*a*) 0.2, (*b*) 0.3, (*c*) 0.4, and (*d*) 0.5 as a function of hydraulic conductivity (k) when subjected to various earthquake magnitude (M) events. The range of hydraulic conductivity is divided into three zones: Zone A—The saturation zone of low permeability having high sand content, Zone B—The transition zone of medium permeability with low sand content, and Zone C—The zone of clean gravel with low permeability. [Color online.]

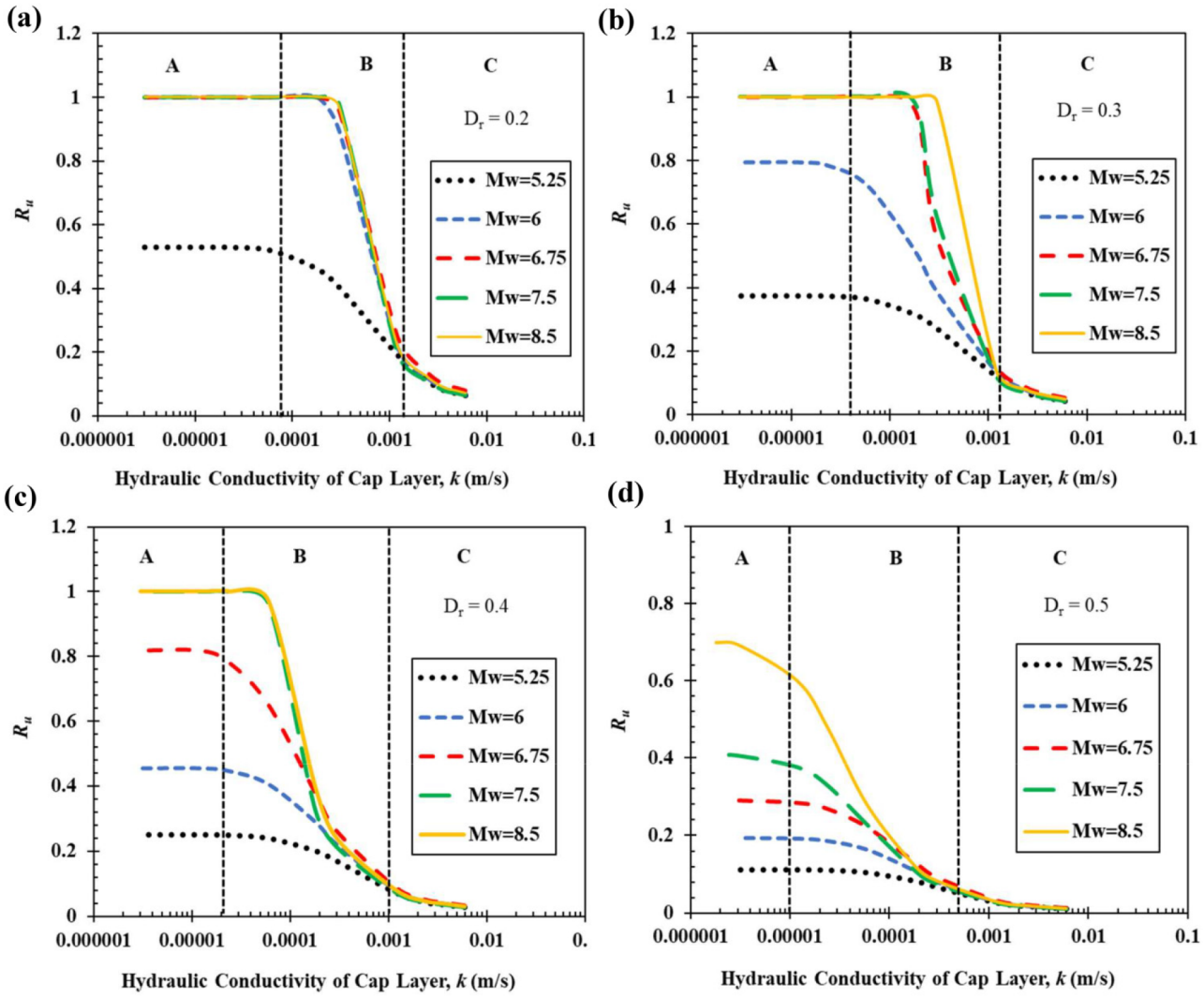

til it reaches a maximum value. The overall variation of R_u with the hydraulic conductivity has been broadly divided into three different zones: Zone C, the zone of clean gravel (sand content below 30% as per Fig. 2) with relatively high permeability (>0.001–0.002 m·s^{-1}), where the value of R_u remains very low (<0.05–0.15) and similar for all earthquake magnitudes. Zone B, the transition zone with medium hydraulic conductivity where the peak R_u increases at a significant rate with decreasing k, and Zone A, the zone of relatively low hydraulic conductivity (<1 × 10^{-5} to 1 × 10^{-4} m·s^{-1}), where peak R_u reaches the highest value and saturates. The distribution of these three zones is depicted in Fig. 4 for all the cases. The boundary between Zone C and Zone B has been drawn roughly at the point where the R_u curves for different earthquake magnitude start to separate as the hydraulic conductivity decreases. The boundary between Zone B and Zone A has been drawn roughly at the point where the R_u curves for all earthquake magnitudes simultaneously attain the maximum or saturation point. The figure shows that the width of these zones depends primarily on the earthquake magnitude and the relative density.

Basically, the variation of R_u with the hydraulic conductivity and the maximum value of R_u largely depends on the earthquake magnitude, soil density, and the gradation. The hydraulic conductivity of the soil matrix depends on the size of D_{10} and some other gradation parameters such as C_u and C_c, which are significantly governed by the percentage of gravel content, sand content, and to some extent on the silt content remaining in the soil matrix. However, D_{10} is the primary factor that controls the k of the soil matrix. As the size of D_{10} decreases with an increase in sand and fines content, the hydraulic conductivity being a direct function of D_{10} gradually decreases causing a reduction in the dissipation of pore water pressure which in turn increases the value of R_u in the

soil matrix. According to Supplementary Table S1, the threshold "k" given by Seed et al. (1976) is attained at D_{10} of 1 mm. the upper end of the transition zone in Fig. 4 is attained at D_{10} of 0.6–0.8 mm and the lower end is attained at the D_{10} of 0.05–0.2 mm, i.e., when the sand content is significantly high. Thus, the amount of sand and fines content plays significant role in controlling the generation of pore pressure during cyclic loading, even causing liquefaction as R_u attains the value of 1.0 at several points within the soil strata.

4.2. Effect of earthquake magnitude

Earthquake magnitude also has a significant effect on the maximum pore pressure ratio that can be generated in the sandy gravel layer. With an increase in the earthquake magnitude, the maximum R_u generated in the sandy gravel layer increases and eventually causes the soil to become liquefied, i.e., R_u reaches a value of 1.0. In addition, the R_u value is higher in the transition zone (Zone B) for a given hydraulic conductivity. These facts can be explained using the excess pore pressure ratio (R_u) versus (N_{eq}/N_l) curve of Seed et al. (1975*a*) given by Fig. 3, which shows that R_u increases with an increase in (N_{eq}/N_l) as, in the case of higher earthquake magnitude, the number of cycles produced by the earthquake (N_{eq}) becomes higher relative to the number of cycles required to cause liquefaction (N_l). In the present study, an increase in earthquake magnitude for a particular soil essentially means an increase in the number of stress cycles, N_{eq}, or N_{eq}/N_l, which naturally causes an increase in the maximum excess pore pressure ratio generated within the gravel layer.

4.3. Effect of soil relative density

Soil relative density has the opposite effect to that of earthquake magnitude. As the relative density increases, the maximum pore pressure decreases for a given earthquake magnitude. It can be observed in Fig. 4 that in the case of low-density soil when D_r is 0.2–0.3, R_u attains a value of 1 when "k" is about 0.001 m·s^{-1} when the magnitude is above 6.75. Whereas in the case of higher soil density when D_r is 0.4 and 0.5 the maximum R_u remains mostly below 1, except for a few cases when the magnitude is greater than 7.5. This is true even when "k" is in the range of 0.0001 to 0.0002 m·s^{-1} where maximum R_u develops. Therefore, with an increase in earthquake magnitude, the gravel layer attains the maximum pore pressure and even liquefies much faster as the soil density decreases from a dense to a loose state. This phenomenon can be explained by the fact that as the density varies from dense to lose, N_l gradually decreases causing the cyclic ratio N_{eq}/N_l to increase significantly. Finally, the compressibility coefficient, m_v, also increases as relative density decreases causing higher-positive pore pressures to be generated due to the increased volumetric compression occurring during cyclic straining.

It can be implied from this parametric study that the generation of pore pressure and the occurrence of liquefaction in a gravelly soil layer during cyclic loading essentially depends on the combination earthquake magnitude, relative density and the hydraulic conductivity, which is basically a function of grain size distribution parameters. Therefore, to predict the generation of the excess pore pressure ratio (R_u) as a function of all these parameters together in a combined form, the term "Liquefaction Resistance Index" (LRI) has been introduced as given by the equation

Fig. 5. Variation of peak excess pore pressure ratio (R_u) with Liquefaction Resistance Index (C_vN_l/N_{eq}). [Color online.]

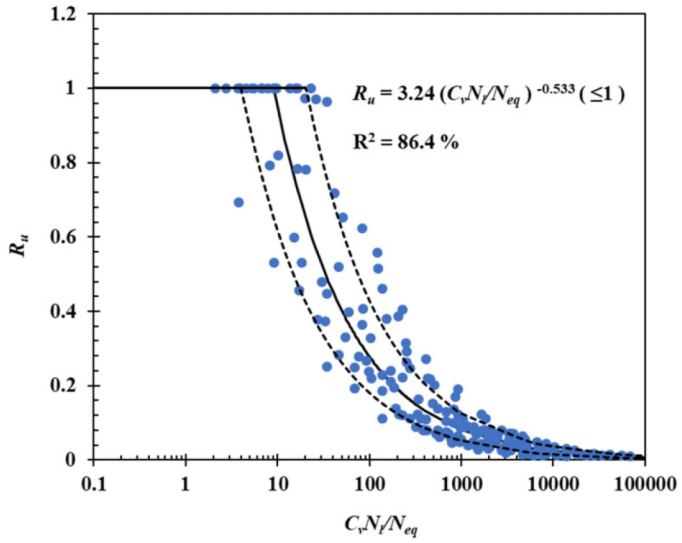

$$\text{(11)}\quad \text{LRI} = \frac{C_v N_l}{N_{eq}}$$

where C_v is the coefficient of consolidation defined by the equation,

$$\text{(12)}\quad C_v = \frac{K}{m_v \gamma_w}$$

which considers both the hydraulic conductivity and relative density through the compressibility coefficient as discussed previously. LRI combines both the earthquake loading and the soil characteristics into one meaningful parameter to predict the excess pore pressure generation during seismic shaking. Based on a complete regression analysis using the results obtained from the parametric analysis with FEQdrain, the best-fit equation for R_u is given by,

$$\text{(13)}\quad R_u = 3.24\left(\frac{C_v N_l}{N_{eq}}\right)^{-0.533} = 3.24(\text{LRI})^{-0.533} \leq 1$$

with standard deviation of 0.43. The correlation coefficient, R^2, associated with this equation is 0.86, which indicates a reasonably good correlation among the variables from a statistical point of view. Based on this formulation, R_u values have been plotted with respect to LRI for the whole data set as shown in Fig. 5. The plot indicates that the data points follow a consistent trend showing good agreement with the best-fit equation obtained from the regression analysis. Along with the best-fit line, the upper- and lower-bound curves (mean ± 1 std. deviation) have been depicted in Fig. 5 by the dashed lines. The equations of upper and lower bound curves are

given by,

$$R_u = 4.98\left(\frac{C_v N_1}{N_{eq}}\right)^{-0.533} = 3.24(\mathrm{LRI})^{-0.533} \leq 1 - \text{Upper Bound} \quad (14)$$

$$R_u = 2.11\left(\frac{C_v N_1}{N_{eq}}\right)^{-0.533} = 3.24(\mathrm{LRI})^{-0.533} \leq 1 - \text{Lower Bound} \quad (15)$$

The upper bound curve estimates higher excess pore pressure ratio compared with the mean curve. Therefore, to evaluate the liquefaction potential of a soil deposit with high factor of safety, the upper bound solution can be used.

5. Results of numerical analysis for confined gravel layer (with overlying cap layer)

As noted by Chen et al. (2018), the presence of a low permeability cap layer on top of a gravelly strata can generate a drainage condition favorable for liquefaction in the underlying gravel layer during earthquake loading. In this regard, the most important and relevant concern is to obtain the threshold hydraulic conductivity of the cap layer at which the pore pressure dissipation begins to be impeded considerably to produce liquefaction in the underlying gravelly soil, i.e., the value of R_u reaches and continues to remain one below this point. Hence to investigate the effect of the overlying cap layer, a 5-m thick sandy gravel layer has been modelled with a 1-m thick cap layer on top. The initial ground water table has been placed at the depth of 2 m from the surface to produce an unsaturated gap of 1 m. This confined 5-m thick sandy gravel deposit has been analyzed for relative densities (D_r) of 0.2, 0.3, 0.4, and 0.5 when subjected to earthquakes ranging in magnitude (M_w) from 5.25 to 8.25 as was done for the unconfined condition. The hydraulic conductivity of the gravel layer has been considered as 0.005 m·s^{-1} and the hydraulic conductivity for the overlying cap layer has been varied from 3×10^{-3} through 3×10^{-7} m·s^{-1} to represent the range of k for a sandy through clayey cap layer. For each of these cases, the maximum R_u has been computed for the sandy gravel stratum as a function the hydraulic conductivity of the overlying cap layer as shown in Fig. 6. The conclusions based on these results are discussed in the following sections.

5.1. Effect of hydraulic conductivity

It can be observed from Fig. 6 that the peak R_u value increases rapidly as the hydraulic conductivity of the cap layer reduces from 1×10^{-3} to 1×10^{-5} m·s^{-1} and attains the value of 1.0 in most of the cases except when the relative density is 0.5 and the earthquake magnitude is below 6.75. As the hydraulic conductivity reduces further to represent a clay cap, the peak R_u value reaches 1.0 in most of the cases indicating the occurrence of liquefaction in the gravel layer, unless the relative density is high ($D_r = 0.5$). Unlike the unconfined case, the rate of increase in R_u and the corresponding maximum value does not significantly depend on the earthquake magnitude and the relative density as the overlying cap layer primarily controls the pore pressure generation by impeding the drainage path. This phenomenon can also be explained by eq. 13 developed in the previous section. For the layered soil strata, the hydraulic conductivity (k) in eq. 13 should be replaced by an equivalent hydraulic conductivity (k_{eq}), which is primarily governed by the overlying cap layer in the present case. Thus, the value of LRI obtained by eq. 12 is low enough to produce liquefaction in the gravel layer.

It should also be noted that the presence of a sandy cap layer can impede the dissipation of pore pressure in the underlying gravel layer even if the hydraulic conductivity of the gravelly stratum is higher than 0.003 m·s^{-1}, so that liquefaction is produced in the gravelly stratum. According to Fig. 6, the threshold hydraulic conductivity of the cap layer necessary to cause liquefaction is in the range of 1×10^{-4} to 1×10^{-5} m·s^{-1} that represents a sandy soil matrix. Hence, the high hydraulic conductivity of the confined gravel layer would not have any significant effect on the generation of excess pore pressure during cyclic shaking as it is controlled by the hydraulic conductivity of the cap layer. For lower hydraulic conductivities in the gravel layer, liquefaction can occur even without the cap layer and peak R_u values consistently remain within the range of 0.8 and 1.0 particularly for higher magnitudes and lower relative densities.

5.2. Effect of earthquake magnitude

The earthquake magnitude has a relatively insignificant effect on the peak excess pore pressure generated during cyclic loading. As the earthquake magnitude increases, the excess pore pressure ratio also increases but not by a significant amount for the low relative density soils involved. Specifically, when the hydraulic conductivity of the overlying cap layer remains below the range of 1×10^{-4} to 1×10^{-5} m·s^{-1}, the effect of magnitude becomes insignificant as the peak R_u value attains a value of 1.0 to indicate the occurrence of liquefaction for almost all the cases where D_r is less than 0.4. But as the relative density increases to 0.5, the effect of magnitude becomes more prominent as the peak R_u value remains below 0.8 when the magnitude is lower than 6.75. Thus, the effect of the earthquake magnitude cannot be observed distinctly in contrast to the behavior of the unconfined gravel layer, except when the relative density is quite high.

5.3. Effect of soil relative density

Similar to the effect of earthquake magnitude, soil relative density also has a very insignificant effect on the peak pore pressure ratio in the gravelly layer during cyclic shaking. When the relative density is low, i.e., D_r is 0.2 and 0.3, the variation in excess pore pressure ratio is insignificant and the peak R_u value reaches unity when the hydraulic conductivity of the cap layer is less than about 1×10^{-4} m·s^{-1}. In the case where D_r is 0.4, the rate of pore pressure generation decreases, and the peak R_u value reaches a value of 1.0 when the hydraulic conductivity of the cap layer is in the range of 1×10^{-5} to 3×10^{-5} m·s^{-1}. But as the relative density increases to 0.5, the peak excess pore pressure does de-

Fig. 6. Variation of computed peak excess pore pressure ratio (R_u) within a 5-m thick confined gravel layer with relative densities (D_r) of (*a*) 0.2, (*b*) 0.3, (*c*) 0.4, and (*d*) 0.5 and the hydraulic conductivity of 0.003 m·s^{-1} as a function of hydraulic conductivity (k) of 0.6-m thick overlying cap layer when subjected to various earthquake magnitude (M_w) events. [Color online.]

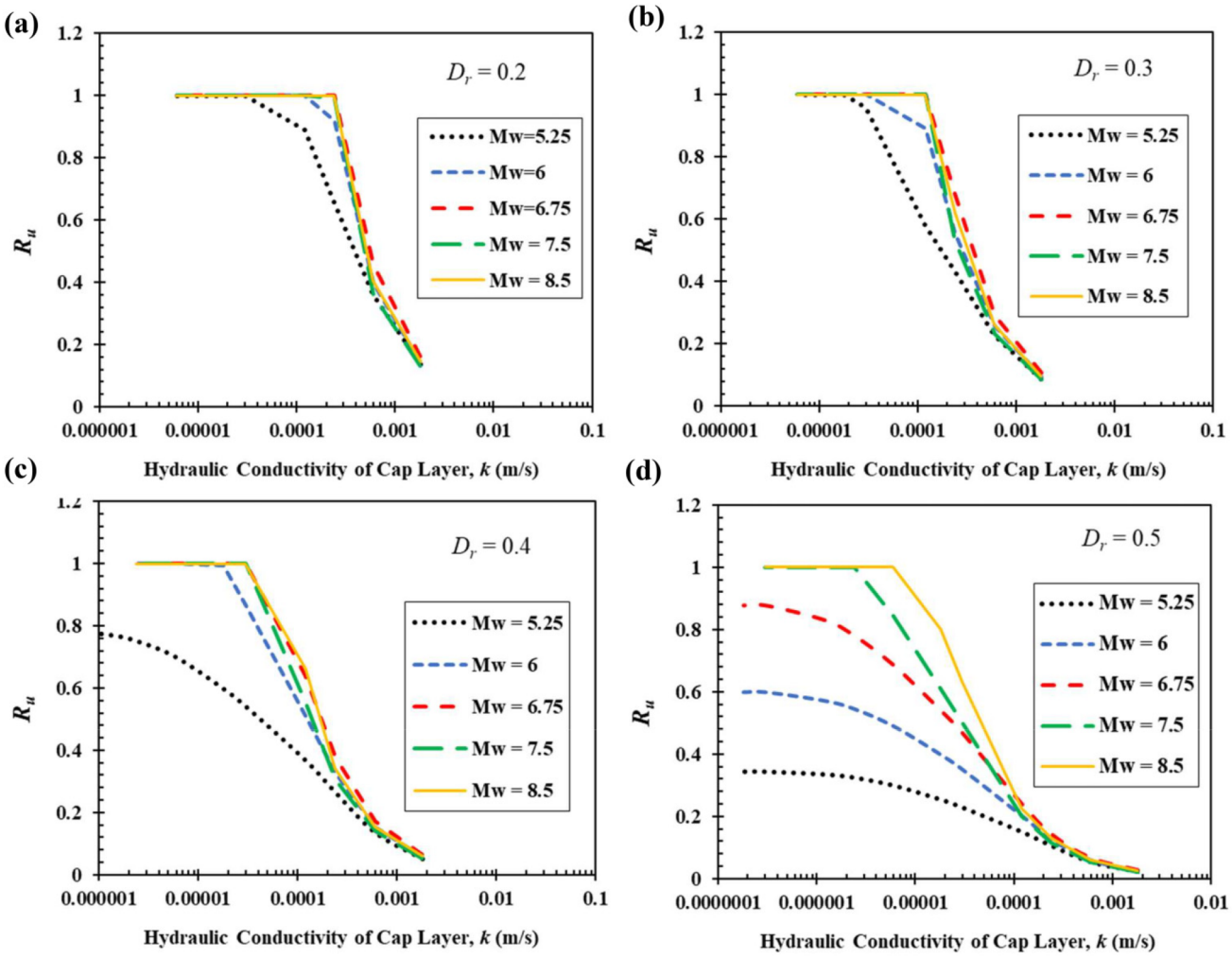

crease considerably as the earthquake magnitude decreases as shown in Fig. 6.

5.4. Effect of gap layer

These analysis results clearly indicate that the peak excess pore pressure ratio can be high, and liquefaction can still occur even when the hydraulic conductivity of the sandy gravel layer is high when a sandy or clayey cap layer impedes drainage in contrast with the unconfined case. However, analysis indicates that the presence of a 1-m thick gap layer above the water table and below the cap layer does not reduce the potential for liquefaction significantly. To further examine this behavior, an additional study was performed keeping the ground water table at the depth of 3 m, i.e., the gap layer being 2-m thick that produced very similar behavior relative to the generation of excess pore pressure ratios in comparison with the 1-m thick gap layer. For the confined condition, the pore pressure generation is primarily governed by the permeability of the cap layer, which impedes drainage, not the unsaturated gap layer. So, the pattern of excess pore pressure ratio remained very similar for the two different gap layer thicknesses. Therefore, the ratio of gap to gravel thicknesses or the ratio of gap to clay thickness did not have any significant effect on the pore pressure generation in the gravel layer. Hence, the analysis results (variation of R_u) for different gap layer thickness have not been shown in separate figures as they are very similar to the results shown in Fig. 6.

6. Variation of excess pore pressure ratio with time and depth

When performing the parametric study, the earthquake loading was applied as a combination of the equivalent number of loading cycles, N_{eq} (Seed and Idriss 1982) and the duration of earthquake shaking, t_d (Seed et al. 1975*b*). Hence, with the variation of hydraulic conductivity, earthquake magnitude and soil relative density, different R_u versus time history results have been obtained for different drainage conditions. In this section, the typical pattern of the variation of excess pore pressure generation with time have been shown to illustrate the process of pore pressure generation for layers with

Fig. 7. Variation of excess pore pressure ratio (R_u) with time various hydraulic conductivity (k), earthquake magnitude, and relative density values of the sandy gravel layer for the unconfined condition: (*a*) $D_r = 0.3$, $M_w = 6.75$, (*b*) $D_r = 0.3$, $M_w = 7.5$, (*c*) $D_r = 0.4$, $M_w = 6.75$, and (*d*) $D_r = 0.4$, $M_w = 7.5$. The plots are shown at depths where the maximum excess pore pressure in the layer eventually develops. [Color online.]

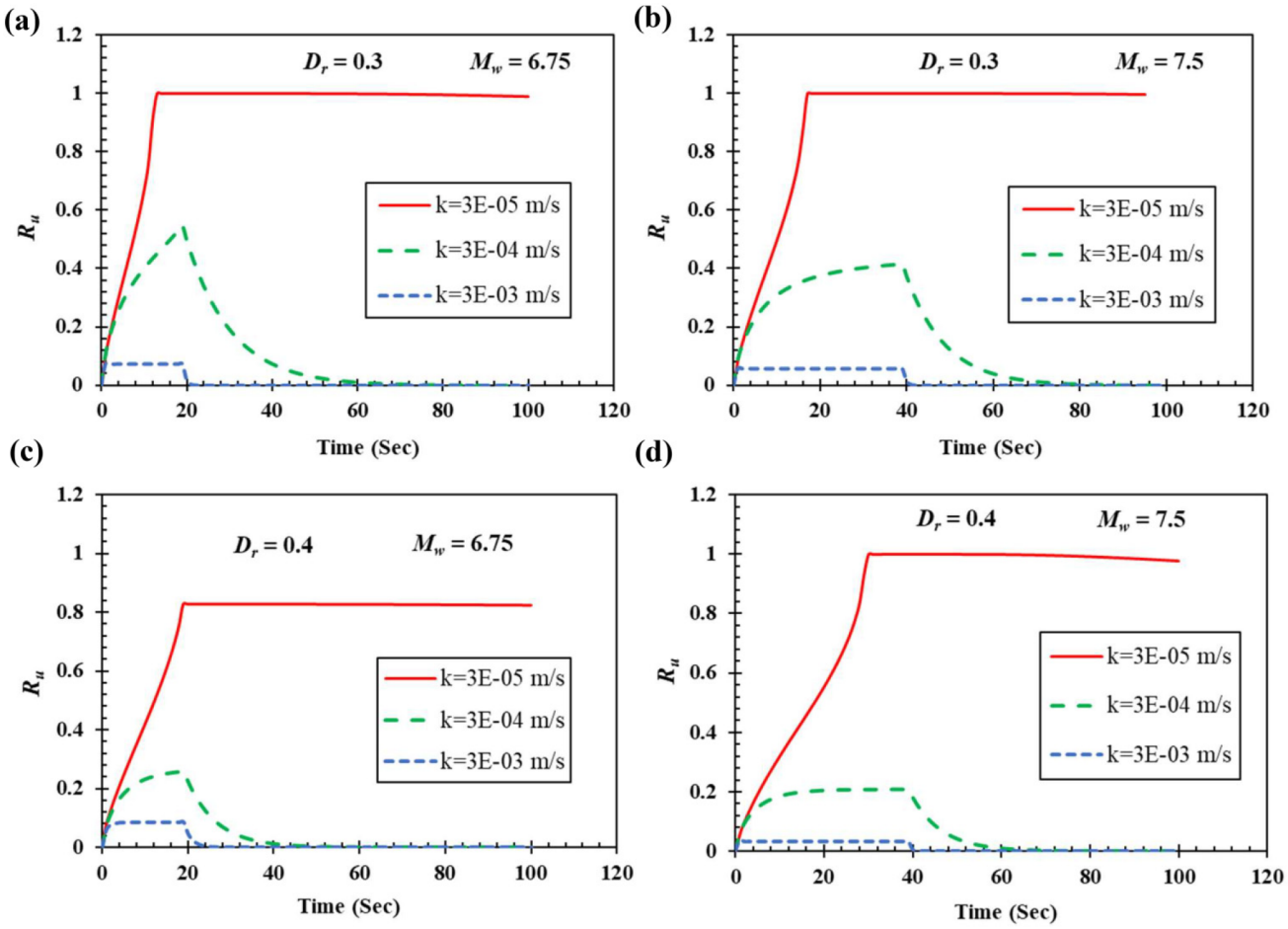

various hydraulic conductivities, earthquake magnitudes and soil relative densities for both the confined and unconfined cases. In addition, the variation of the peak R_u with depth for the entire time span has also been obtained and the typical results are shown along with the time history results.

6.1. Results for unconfined sandy gravel (without cap layer)

The typical variations of R_u with time and depth for the unconfined condition are shown in Figs. 7 and 8, respectively. The plot in Fig. 7 is based on the values of R_u at depths where the maximum R_u eventually develops. Figure 7 shows that as the hydraulic conductivity decreases, the maximum pore pressure ratio gradually increases, and the time required to reach the maximum value also decreases gradually. This happens because the dissipation of pore pressure reduces with the decrease in hydraulic conductivity causing the soil to liquefy within a shorter span of time. For sandy gravel layers with higher hydraulic conductivities, when excess pore pressure ratios develop, they tend to dissipate rapidly and decrease to zero. But as hydraulic conductivity decreases and liquefaction takes place, the excess pore pressure ratio remains relatively high with a residual value after the liquefaction. The time history results shown in Fig. 7 have been obtained for the earthquake magnitudes of 6.75 and 7.5 and relative densities of 0.3 and 0.4. Although the variation of earthquake loading and the relative density changes the values of the maximum R_u and the time of liquefaction, the overall pattern of the R_u versus time curves remains very similar for all the cases.

Figure 8 shows that the development of the maximum R_u with depth is generally quite consistent over the whole sandy gravel stratum. R_u versus depth results have been obtained for similar variations of hydraulic conductivity for earthquake magnitudes of 6.75 and 7.5 and relative densities of 0.3 and 0.4. Figure 8 shows that as the hydraulic conductivity decreases, the maximum value of R_u gradually increases throughout the depth and eventually reaches a value of 1.0 indicating liquefaction. The generation of excess pore pressure is relatively low in the upper 0.5 m of the layer because dissipation of pore pressure is more pronounced in this zone compared with the deeper zones in the layer. Similar behavior of pore pressure generation with depth is observed for all

Fig. 8. Variation of peak excess pore pressure ratio (R_u) with depth for various hydraulic conductivity (k) earthquake magnitude and relative density values of the sandy gravel layer for the unconfined condition: (a) $D_r = 0.3$, $M_w = 6.75$, (b) $D_r = 0.3$, $M_w = 7.5$, (c) $D_r = 0.4$, $M_w = 6.75$, and (d) $D_r = 0.4$, $M_w = 7.5$. The plots show the peak R_u values along the depth for the entire time. [Color online.]

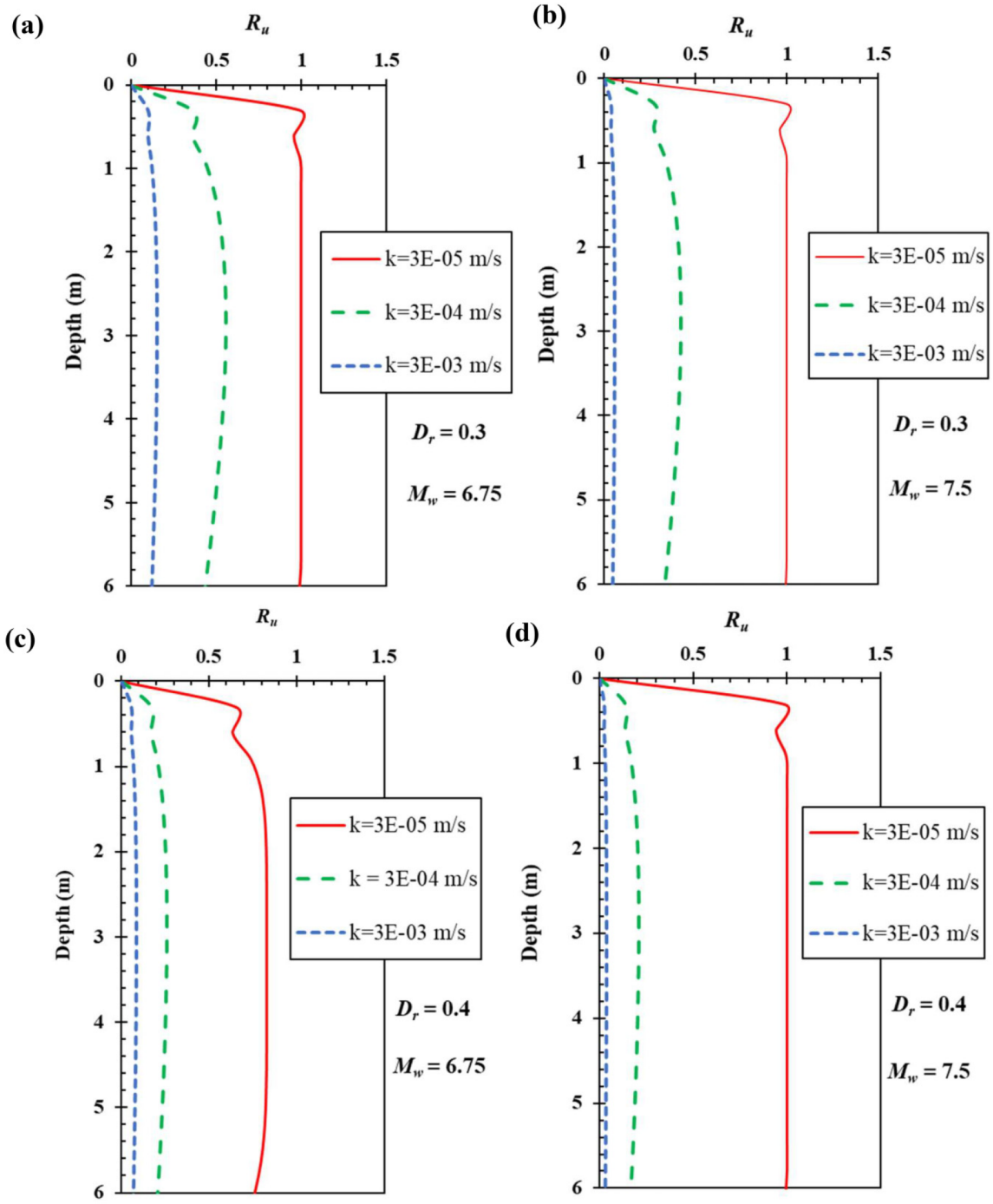

the cases of earthquake magnitude and relative density considered in the study.

6.2. Results for confined sandy gravel (with cap layer)

The typical variation of R_u with time and depth for the confined sandy gravel layer with an overlying lower permeability cap layer is shown in Figs. 9 and 10, respectively. Figure 9 shows that the maximum value of R_u reaches a value of 1.0 even for higher hydraulic conductivity values and the time to liquefaction gradually decreases as the hydraulic conductivity increases, which contrasts with the case of the unconfined gravelly stratum. As the hydraulic conductivity increases, the pore pressure dissipates rapidly in the upward direction but increases just below the boundary of the cap layer to cause

Fig. 9. Variation of excess pore pressure ratio (R_u) with time for confined gravel layers with various hydraulic conductivity (k), earthquake magnitude, and relative density values: (*a*) $D_r = 0.3$, $M_w = 6.75$, (*b*) $D_r = 0.3$, $M_w = 7.5$, (*c*) $D_r = 0.4$, $M_w = 6.75$, and (*d*) $D_r = 0.4$, $M_w = 7.5$. The time histories are plotted for the depth where the maximum R_u eventually develops. [Color online.]

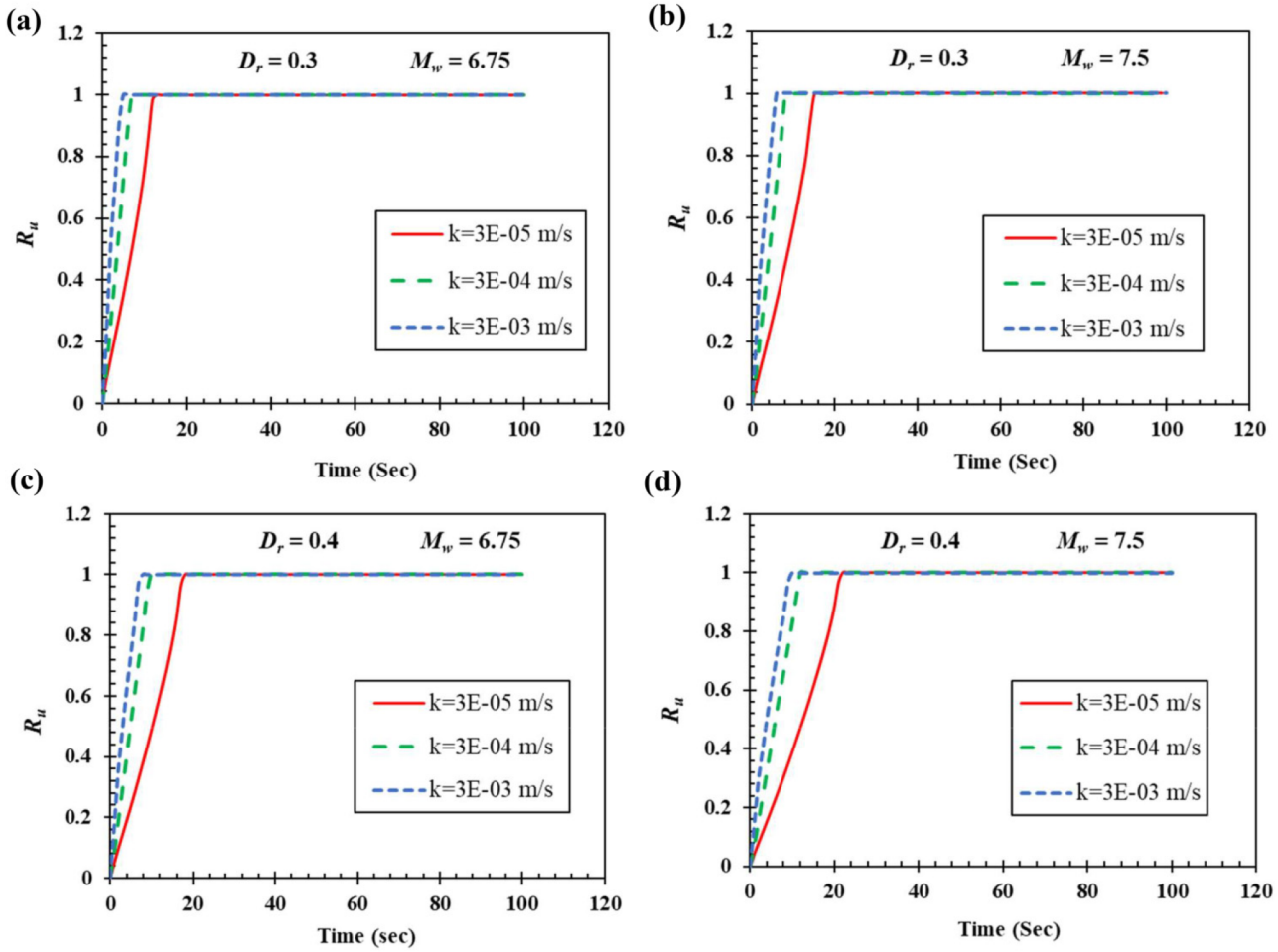

liquefaction even earlier than for the lower hydraulic conductivity condition. These results have been plotted for magnitudes of 6.75 and 7.5 and for relative densities of 0.3 and 0.4 as in the unconfined case; however, similar behavior with respect to pore pressure generation with little variation in the time required to cause liquefaction is observed for all the earthquake magnitudes and relative densities considered in this study.

As in the previous case for the unconfined case, R_u versus depth has been plotted in Fig. 10 for earthquake magnitudes of 6.75 and 7.5 and for relative densities of 0.3 and 0.4 for the same variations of hydraulic conductivity in the gravel. Figure 9 shows that the maximum R_u develops just beneath the clay layer when the hydraulic conductivity is about 3×10^{-3} m·s^{-1} and then drops to a value between 0.3 and 0.5 at depths below about 1 m. But as the hydraulic conductivity decreases, the pore pressure dissipation also decreases such that liquefaction develops within the entire depth of the profile. However, as the relative density increases, i.e., when D_r is at 0.4, the peak R_u along the depth gradually decreases as compared with the looser gravelly soil ($D_r = 0.3$).

Similar analyses were performed for the case with an unsaturated gap layer beneath the impermeable clay layer. The results show that, despite the gap layer, the peak excess pore pressure ratio reaches 1.0 beneath the overlying cap layer because water flows upward from the deeper layers and accumulates below the cap. Therefore, a similar pattern develops for the R_u versus time and depth curves compared with those shown in Figs. 9 and 10. Thus, the potential for liquefaction remains considerably high just beneath the cap even though the gravelly layer has a high hydraulic conductivity.

Conclusions

Based on the field case histories and the numerical study results, the following conclusions can be drawn regarding the effect of hydraulic conductivity on the liquefaction of gravelly soil.

1. Gravel layers with hydraulic conductivities greater than 0.004 m·s^{-1} (D_{10} of 1 mm) are expected to dissipate excess pore pressures as fast as they are generated by an earthquake provided there is no low hydraulic conductiv-

Fig. 10. Variation of peak excess pore pressure ratio (R_u) with depth confined gravel layers with for various hydraulic conductivity (k) earthquake magnitude and relative density values: (a) $D_r = 0.3$, $M_w = 6.75$, (b) $D_r = 0.3$, $M_w = 7.5$, (c) $D_r = 0.4$, $M_w = 6.75$, and (d) $D_r = 0.4$, $M_w = 7.5$. The plots show the peak R_u along the depth for the entire time. [Color online.]

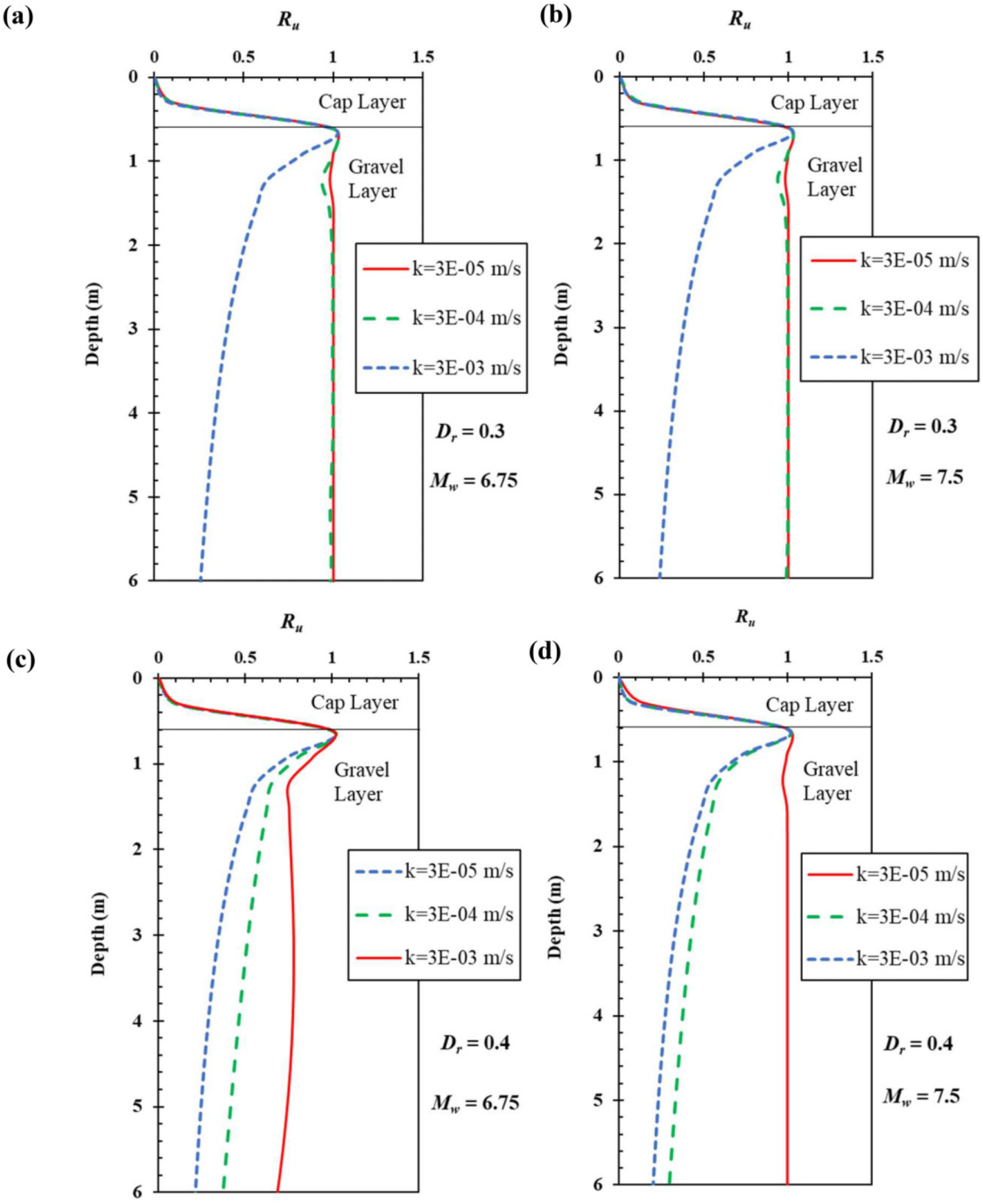

ity boundary layer. However, hydraulic conductivities for gravels that have liquefied historically have typically been significantly less than 0.004 m·s^{-1}, which is more typical of the hydraulic conductivity of sands.

2. Gravels that have liquefied historically generally had sand contents greater than 20% and more typically greater than 30%. As the sand content exceeds about 30%, the sand will likely fill the void space in the gravel and reduce the hydraulic conductivity from that for gravel to that of sand.
3. The sand content in a sandy gravel mixture reduces the hydraulic conductivity of the overall soil deposit, which in turn increases the potential for liquefaction. Because of the lower hydraulic conductivity and reduced potential for dissipation, shaking can generate significant pore pressures, and produce liquefaction even without the presence of an impermeable cap layer.
4. Numerical analyses of pore pressure generation in unconfined sandy gravel layers indicate that the peak excess

pore pressure ratio (R_u) for all earthquake magnitudes remains below 0.05–0.15 when the hydraulic conductivity is in the range of 0.001–0.002 m s^{-1} (D_{10} of 0.6–0.8 mm). R_u increases rapidly in the transition zone as the hydraulic conductivity varies from 0.001–0.002 m·s^{-1} (D_{10} of 0.6–0.8 mm) to 0.0001–0.00001 m·s^{-1} (D_{10} of 0.05–0.2 mm). The zone of high R_u values tends to be relatively uniform over the whole thickness of the gravel layer. Numerical analyses also indicate that earthquake magnitude and relative density have significant effects on the pore pressure generation in the unconfined gravel layers. The peak excess pore pressure ratio increases with higher earthquake magnitude, but decreases with the increase in relative density.

5. For unconfined gravel layers, peak R_u values can be reasonably predicted as a function of hydraulic conductivity, volumetric compressibility, the equivalent number of loading cycles of the earthquake, and the minimum number of cycles required to cause liquefaction.
6. In the case of a confined sandy gravel stratum, the presence of a low permeability cap layer, overlying the gravelly layer, impedes drainage, and can lead to liquefaction even for gravels with hydraulic conductivities greater than 0.004 m·s^{-1} for relative densities less than 0.4. However, the zone of liquefaction is typically concentrated within a metre or so below the impermeable cap due to the upward flow of water from the underlying gravel while peak R_u values are typically less than 0.5 at depths below the interface. It was also observed from the numerical study that the earthquake magnitude and the relative density have relatively insignificant effects on the excess pore pressure generation within the gravel stratum.
7. Based on numerical analyses of confined gravelly strata with varying hydraulic conductivities below a low permeability cap layer, it was observed that as the hydraulic conductivity of the cap layer goes below the range of fine-grained sand, i.e., 3×10^{-4} to 3×10^{-5} m·s^{-1}, the cap layer impedes the dissipation of excess pore pressure and allows liquefaction in the gravelly stratum. Hence, the presence of an impermeable clay cap or a low permeability sandy layer can restrict the drainage path to produce liquefaction even in coarse grained gravelly soil. Although the present study is based on level ground condition with no effect of lateral boundary condition assuming only vertical drainage, the role of cap layer would still be similar in the case of gently sloping ground where both lateral and vertical deformations and boundary conditions are significant. However, specific analysis may be required to estimate excess pore pressure ratio accounting for the effects of both lateral and vertical deformation.
8. Results of the numerical analyses for the confined case show that the presence of an unsaturated gap layer between an impermeable clay cap and the water table does not have any significant effect on the generation of excess pore pressure. Even after dissipating into the unsaturated zone, high R_u values still develop below the clay cap as water accumulates from upward flow in the underlying gravel.

Acknowledgements

Funding for this study was provided by grant G16AP00108 from the US Geological Survey Earthquake Hazard Reduction Program and grant CMMI-1663546 from the National Science Foundation. This funding is gratefully acknowledged. However, the opinions, conclusions and recommendations in this paper do not necessarily represent those of the sponsors.

Article information

History dates

Received: 15 October 2021
Accepted: 4 May 2022
Accepted manuscript online: 11 May 2022
Version of record online: 13 October 2022

Data availability

Some or all data, models, or code that support the findings of this study are available from the corresponding author upon request. These data include input files used in the FEQDrain analyses.

Author information

Author ORCIDs

Jashod Roy https://orcid.org/0000-0003-0854-3790
Kyle M. Rollins https://orcid.org/0000-0002-8977-6619

Supplementary material

Supplementary data are available with the article at https://doi.org/10.1139/cgj-2021-0579.

References

Andrus, R.D. 1994. In situ characterization of gravelly soils that liquefied in the 1983 Borah Peak Earthquake. Doctoral Dissertation, Civil Engineering Dept. University of Texas at Austin, USA.

Andrus, R.D., and Stokoe, K.H., II 2000. Liquefaction resistance of soils from shear-wave velocity. Journal of Geotechnical and Geoenvironmental Engineering. **11**(1015): 1015–1025. doi:10.1061/(ASCE)1090-0241(2000)126.

Andrus, R.D., Stokoe, K.H., II, and Chung, R.M. 1999. Draft guidelines for evaluating liquefaction resistance using shear wave velocity measurements and simplified procedures, National Institute of Standards and Technology, Gaithersburg, MD.

Athanasopoulos-Zekkos, A., Zekkos, D., Rollins, K.M., Hubler, J., Higbee,, J., and Platis,, A. 2019. Earthquake performance and characterization of gravel-size earthfills in the ports of Cephalonia, Greece, following the 2014 Earthquakes. In Earthquake Geotechnical Engineering for Protection and Development of Environment and Constructions. Proceedings of the 7th International Conference on Earthquake Geotechnical Engineering. Taylor and Francis. pp. 1212–1219.

Banerjee, N.G. 1979. Cyclic behavior of dense coarse-grained materials in relation to the seismic stability of dams. UCB/EERC-79/13, https://nisee.berkeley.edu/elibrary/eerc_reports.html. June, 1979.

Bolt, B.A. 1973. Duration of strong ground motion. In 5th World Conference on Earthquake Engineering, Month - June. Vol. **292**, pp.Rome 25–29.

Cao, Z., Youd, T., and Yuan, X. 2013. Chinese dynamic penetration test for liquefaction evaluation in gravelly soils. Journal of Geotechnical and Geoenvironmental Engineering. **139**(8): 1320–1333. doi:10.1061/(ASCE)GT.1943-5606.0000857.

Carman, P.C. 1936. Fluid flow through granular beds. Transactions, Institution of Chemical Engineers, London, **15**: 150–166.

Carman, P.C. 1956. Flow of Gases through Porous Media. Butterworths Scientific Publications, London.

Carrier, W.D. 2003. Goodbye, hazen; hello, kozeny-carman. Journal of Geotechnical and Geoenvironmental Engineering. **129**(11):1054–1056.

Chang, W.J. 2016. Evaluation of liquefaction resistance for gravelly sands using gravel content–corrected shear-wave velocity. Journal of Geotechnical and Geoenvironmental Engineering. **142**(5): 04016002. doi:10.1061/(ASCE)GT.1943-5606.0001427.

Chang, W.J., Chang, C.W., and Zeng, J.K. 2014. Liquefaction characteristics of gap-graded gravelly soils in K0 condition. Soil Dynamics and Earthquake Engineering. **56**: 74–85. doi:10.1016/j.soildyn.2013.10.005.

Chen, L., Yuan, X., Cao, Z., Sun, R., Wang, W., and Liu, H. 2018. Characteristics and triggering conditions for naturally deposited gravelly soils that liquefied following the 2008 Wenchuan M_w 7.9 earthquake, China. Earthquake Spectra, **34**(3): 1091–1111. doi:10.1193/032017EQS050M.

Chu, B.L., Hsu, S.C., Lai, S.E., and Chang, M.J. 2000. "Soil Liquefaction Potential Assessment of the Wu feng Area after the 921 Chi-Chi Earthquake." Report of National Science Council (in Chinese).

Coulter, H.W., and Migliaccio, R.R. 1966. Effect of the Earthquake of March 22, 1964, at Valdez, Alaska. U.S. Geological Survey Professional Paper 542-C. 36 p.

Cubrinovski, M, Bray, JD, de la Torre, C., Olsen, M., Bradley, B.A. Chiaro, G., et al. 2017. Liquefaction effects and associated damages observed at the Wellington centreport from the 2016 Kaikōura earthquake. Bulletin of New Zealand Society for Earthquake Engineering. **50**(2): 152–173. doi:10.5459/bnzsee.50.2.152-173.

DeAlba, P., Chan, C.K., and Seed, H.B. 1975. Determination of soil liquefaction characteristics by large scale laboratory tests. Earthquake Engineering Research Center, Report No. EERC 75-14.

DeJong, J.T., Ghafghazi, M., Sturm, A.P., Wilson, D.W., den Dulk, J. Armstrong, R.J., et al. 2017. Instrumented Becker penetration test. I: equipment, operation, and performance. Journal of Geotechnical and Geoenvironmental Engineering. **143**(9): 1–9. doi:10.1061/(ASCE)GT.1943-5606.0001718. doi:10.1061/(ASCE)GT.1943-5606.0001717.

Evans, M.D., and Seed, H.B. 1987. Undrained cyclic triaxial testing of gravels: the effect of membrane compliance. College of Engineering, University of California, USA.

Evans, M.D., and Zhou, S. 1995. Liquefaction behavior of sand-gravel composites. Journal of Geotechnical Engineering, ASCE, **121**(3): 287–298. doi:10.1061/(ASCE)0733-9410(1995)121:3(287).

Harder, L.F., and Seed, H.B. 1986. Determination of penetration resistance for coarse-grained soils using the Becker hammer drill. College of Engineering, University of California, USA.

Hatanaka, M., Uchida, A., and Ohara, J. 1997. Liquefaction characteristics of a gravelly fill liquefied during the 1995 Hyogo-ken Nanbu earthquake. Soils and Foundations. **37**(3): 107–115. doi:10.3208/sandf.37.3_107.

Hazen, A. 1892. Some physical properties of sands and gravels, with special reference to their use in filtration. 24th Annual Report, Massachusetts State Board of Health, Pub.Doc. No. **34**: 539–556.

Hubler, J.F., Athanasopoulos-Zekkos, A., and Zekkos, D. 2017. Monotonic, cyclic, and postcyclic simple shear response of three uniform gravels in constant volume conditions. Journal of Geotechnical and Geoenvironmental Engineering. **143**(9): 04017043. doi:10.1061/(ASCE)GT.1943-5606.0001723.

Hynes, M.E. 1988. Pore pressure generation characteristics of gravel under undrained cyclic loading. Vol. **1**, University of California, Berkeley.

Idriss, I.M. 1999. ''Presentation notes: an update of the seed-idriss simplified procedure for evaluating liquefaction potential. Proc., TRB Workshop on New Approaches to Liquefaction Anal., Publ. No. FHWARD-99-165, Federal Highway Administration, Washington, D.C.

Idriss, I.M., and Boulanger, R.W. 2008. Monograph MNO-12. Earthquake Engineering Research Institute. Oakland, CA.

Ishihara, K. 1985. Stability of natural deposits during earthquakes. Proc., 11th Int. Conf. on Soil Mech. and Found. Eng., **1**, 321–376.

Kayen, R., Moss, R.E.S., Thompson, E.M., Seed, R.B., Cetin, K.O., Der Kiureghian,, A., Tanaka, Y., and Tokimatsu, K. 2013. Shear-wave velocity-based probabilistic and deterministic assessment of seismic soil liquefaction potential. Journal of Geotechnical Engineering. doi:10.1061/(ASCE)GT.1943-5606.0000743.

Kokusho, T., and Yoshida, Y. 1997. SPT N-value and S-wave velocity for gravelly soils with different grain size distribution. Soils and Foundations **37**(4): 105–113.

Kokusho, T., Hara, T., and Hiraoka, R. 2004. Undrained shear strength of granular soils with different particle gradations. Journal of Geotechnical and Geoenvironmental Engineering. **130**(6): 621–629. doi:10.1061/(ASCE)1090-0241(2004)130:6(621).

Kokusho, T., Tanaka, Y., Kawai, T., Kudo, K., Suzuki, K., Tohda, S., and Abe, S. 1995. Case study of rock debris avalanche gravel liquefied during 1993 Hokkaido-Nansei-Oki earthquake. Soils and Foundations. **35**(3): 83–95. doi:10.3208/sandf.35.83.

Kozeny, J. 1927. Ueber kapillare leitung des wassers im boden. Sitzungsber Akad. Wiss., Wien, **136**(2a): 271–306.

Lee, K.L., and Albaisa, A. 1974. Earthquake induced settlements in saturated sands. ASCE, Journal of Geotechnical Engineering Division. **100**(GT4): 387–406. doi:10.1061/AJGEB6.0000034.

Lopez de San Román-Blanco, B. 2003. Dynamics of gravel and mixed sand and gravel beaches. Unpublished PhD thesis, Imperial College, University of London.

Lopez, S., Vera-Grunauer, X., Rollins, K., and Salvatierra, G. 2018. Gravelly soil liquefaction after the 2016 ecuador earthquake. Proc. Conf. on Geotechnical Earthquake Engineering and Soil Dynamics V: Liquefaction Triggering, Consequences and Mitigation, Month - June. Reston, VA. 273–285.

Mason, T., Voulgaris, G., Simmonds, D.J., and Collins, M.B. 1997. Hydrodynamics and sediment transport on composite (mixed sand /shingle) and sand beaches: a comparison. In Coastal Dynamics' **97**(pp. 48–57). ASCE, Plymouth, UK.1997.

Maurenbrecher, P.M., Den Outer, A., and Luger, H.J. 1995. Review of geotechnical investiga-tions resulting from the Roermond April 13, 1992 earthquake., Proc. 3rd Int. Conf. on Recent Advances in Geotech. Earthquake Engineering and Soil Dynamics. 645–652.

McCulloch, D. S., and Bonilla, M. G. 1970. Effects of the earthquake of March 27, 1964, on the Alaska Railroad. US Government Printing Office.

Milan, V., and Andjelko, S. 1992. Determination of hydraulic conductivity of porous media from grain-size composition. **986**, 551.49.

Nikolaou, S., Zekkos, D., Assimaki, D, and Gilsanz, R. 2014. GEER/EERI/ATC Earthquake Reconnaissance January 26th/February 2nd 2014 Cephalonia, Greece Events, Version 1.

Odong, J. 2007. Evaluation of empirical formulae for determination of hydraulic conductivity based on grain-size analysis. Journal of American Science. **3**(3): 54–60.

Pestana, J.M., Hunt, C.E., and Goughnour, R.R. 1997. FEQDrain: A Finite Element Computer Program for the Analysis of the Earthquake Generation and Dissipation of Pore Water Pressure in Layered Sand Deposits with Vertical Drains. Report No. EERC 97-17, Earthquake Engineering Research Center, University of California at Berkeley, CA.

Rollins, K.M., Amoroso, S., Milan, G., Minerelli, L., Vassallo, M., and Di Giulio, G. 2020. Gravel liquefaction assessment using the dynamic cone penetration test based on field perfor-mance from the 1976 Friuli earthquake. Journal of Geotechnical and Geoenvironmental Engineering. ASCE. doi:https://DOI.org/10.1061/(ASCE)GT.1943-5606.0002252.

Rollins, K.M., Roy, J., Athanasopoulos-Zekkos, A., Zekkos, D., Amoroso, S., and Cao, Z. 2021. A new dynamic cone penetration test–based procedure for liquefaction triggering assessment of gravelly soils. Journal of Geotechnical and Geoenvironmental Engineering. **147**(12): 04021141. doi:10.1061/(ASCE)GT.1943-5606.0002686.

Seed, H.B., and Idriss, I.M. 1970. Soil moduli and damping factors for dynamic response analyses. Rep. No. *EERC 70-10*, Earthquake Engi-

neering Research Center, Univ. of California at Berkeley, Berkeley, California.

Seed, H.B., and Idriss, I.M. 1982. Ground motions and soil liquefaction during earthquakes. Earthquake Engineering Research Institute, University of California, Berkeley.

Seed, H.B., Idriss, I.M., Makdisi, F., and Banerjee, N. 1975b. Representation of irregular stress time histories by equivalent uniform stress series in liquefaction analyses. Earthquake Engineering Research Center, University of California, Berkeley, Report No. EERC 75-29.

Seed, H.B., Martin, P.P., and Lysmer, J. 1975a. The generation and dissipation of pore water pressure changes during soil liquefaction. Earthquake Engineering Research Center, University of California, Berkeley, Report No. UCB/EERC 75-26.

Seed, H.B., Martin, P.P., and Lysmer, J. 1976. The generation and dissipation of pore water pressure changes during soil liquefaction. Journal of the Geotechnical Engineering Division. **102**(4): 323–346. doi:10.1061/AJGEB6.0000258.

Seed, H.B., Wong, R.T., Idriss, I.M., and Tokimatsu, K. 1986. Moduli and damping factors for dynamic analyses of cohesionless soils. Journal of the Geotechnical Engineering. **112**(11): 1016–1032. doi:10.1061/(ASCE)0733-9410(1986)112:11(1016).

She, K., Horn, D.P., and Canning, P. 2006. Porosity and hydraulic conductivity of mixed sand-gravel sediment. Flood and Coastal Risk Management, At York, 1–16.

Sirovich, L. 1996a. Repetitive liquefaction at gravelly site and liquefaction in overconsolidated sands. Soils and Foundations. **4**(36): 23–34. doi:10.3208/sandf.36.4_23.

Sirovich, L. 1996b. In-situ testing of repeatedly liquefied gravels and liquefied overconsolidated sands. Soils and Foundations. **4**(36): 35–44. doi:10.3208/sandf.36.4_35.

Tokimatsu, K., and Yoshimi, Y. 1983. Empirical correlation of soil liquefaction based on SPT N-value and fines content. Soils and Foundations. **23**(4): 56–74.

Wang, W.S. 1984. Earthquake damages to earth dams and levees in relation to soil liquefaction and weakness in soft clays. In Proc. Intl. Conf. on Case Histories in Geotech. Eng., **1**, 511–521.

Wong, T., Seed, H., and Chan, C. 1974. Liquefaction of gravelly soils under cyclic loading conditions. University of California, Earthquake Engineering Research Center, Berkeley, EERC Report, (74-11).

Yegian, M.K., Marciano, E.A., and Ghahraman, V.G. 1988. Integrated seismic risk analysis for earth dams. Earthquake hazard mitigation program. National Science Foundation, Alexandra, VA.

Youd, T.L., Harp, E.L., Keefer, D.K., and Wilson, R.C. 1985. The Borah Peak, Idaho Earth-quake of October 29, l983-Liquefaction. Earthquake Spectra, **2**, 71–90.

Zhou, Y. G., Xia, P., Ling, D. S., and Chen, Y. M. 2020. Liquefaction case studies of gravelly soils during the 2008 Wenchuan earthquake. Engineering Geology. **274**: 105691.